Optik 140 (2017) 749–761

Contents lists available at ScienceDirect

Optik

journal homepage: www.elsevier.de/ijleo

Original research article

Segmentation and classification of melanoma and benign skin lesions

Fekrache Dalila [a], Ameur Zohra [a], Kasmi Reda [b,c,*], Cherifi Hocine [d]

[a] Laboratory of Analysis and Modeling of the Random Phenomena (L.A.M.P.A), Departement of Electronics, Faculty of Electronic Engineering and Computer Science, University of Mouloud Mammeri (U.M.M.T.O.), BP 17 RP, Tizi-Ouzou, Algeria
[b] Laboratory of Industrial Technology and Information (LTII), University of Bejaia, Bejaia, Algeria
[c] Electrical Engenieering, University of Bouira, Bouira, Algeria
[d] Laboratory of Electronics, Informatics and Image (LE2I), University of Bourgogne, Dijon, France

ARTICLE INFO

Article history:
Received 24 September 2016
Received in revised form 16 April 2017
Accepted 23 April 2017

Keywords:
Computer-aided diagnosis
Melanoma
Segmentation
Ant colony
Feature extraction
Dermoscopy
K-Nearest Neighbor
Neural network

ABSTRACT

The incidence ofmalignant melanoma has been increasing worldwide. An efficient non-invasive computer-aided diagnosis (CAD) is seen as a solution to make identification process faster, and accessible to a large population. Such automated system relies on three things: reliable lesion segmentation, pertinent features' extraction and good lesion classifier. In this paper, we propose an automated system that uses an Ant colony based segmentation algorithm, takes into consideration three types of features to describe malignant lesion:geometrical properties, textureand relative colors from which pertinent ones are selected, and uses two classifiers K-Nearest Neighbor (KNN) and Artificial Neural Network (ANN). The objective of this paper is to test the efficiency of the proposed segmentation algorithm, extract most pertinent features that describe melanomas and compare the two classifiers. Our automated system is tested on 172 dermoscopic images where 88 are malignant melanomas and 84 benign lesions. The results of the proposed segmentation algorithm are encouraging as they gave promising results. 12 features seem to be sufficient to detect malignant melanoma. Moreover, ANN gives better results than KNN.

1. Introduction

Malignant melanoma is the inhomogeneous growth of skin cells caused by DNA break. It is the deadliest skin cancer [1]. Worldwide, in 2012, there were about 160 000 cases of malignant melanoma and about 41 000 deaths. The statistics show the incidence of skin cancer has been rising in many countries for the last decades [2]. In the United States, there were an estimated 73 870 new cases and 9 940 deaths from melanoma in 2015 [3].

Dermatologists use many procedures to distinguish malignant melanomas from benign lesions such as ABCD rule [4,5], seven point checklist [6], three point checklist [7] or CASH algorithm [8]. These methods are based on three types of features' lesion:geometrical, color, structural and texture. To increase the efficiency and makethe diagnosis process faster, accessible for non expert practitioner, many researchers have been attempting to develop a non-invasive imaging computerized diagnosis. Theselection of relevant features is a crucial step in an automatic diagnosis. Numerous algorithms have been proposed to distinguish malignant melanoma from benign lesions. Rastgoo et al. [9] proposed an automatic algorithm to differentiate

* Corresponding author at: Laboratory of Industrial Technology and Information (LTII), University of Bejaia, Bejaia, Algeria.
E-mail address: rdkasmi@gmail.com (K. Reda).

http://dx.doi.org/10.1016/j.ijleo.2017.04.084
0030-4026/

melanoma from dysplastic nevi. Three classifiers were used and three types of features wereextracted including shape, color and texture of the lesion. The features were tested individually and combined. The paper reported that using texture features and random forest achieved the highest sensitivity 98% and specificity 70%. Kasmi et al. [10] automated the ABCD rule. The algorithm was tested on 200 dermoscopic images and achieved an overall accuracy of 94.0%. Ferris et al. [11] extracted 54 features including border irregularity, eccentricity, length of major and minor axes, and color histogram properties. They tested their algorithm on a set of 159 dermoscopic images (39 melanomas and 120 benign lesions), the decision forest classifier achieved sensitivity of 97.4% and the specificity of 44.2%. LeAnder et al. in [12] extracted relative-color from dermoscopic images to differentiate automatically among malignant melanoma.

In this paper, we propose an approach to differentiate malignant melanoma from benign lesions. First, the lesions are automatically segmented using Ant Colony Optimization, then three types of features are extracted based on the geometrical properties of the lesion as described by the ABCD rule, textures features calculating first-order histogram based features, and relative color. 112 features are extracted and 12 pertinent attributes are selected using Relief algorithm. Two classifiers are used, the K Nearest Neighbor (KNN) and a Neural Network (NN).

The remainder of the paper is structured as follow. In Section 2, a novel algorithm is proposed to skin lesion segmentation based on Ant Colony Optimization. Feature extraction and selection inspired from ABCD rule, including geometrical properties, texture and relative colors are described in Section 3. In the fourth section classification, experimental method and results are reported and discussed. Finally, conclusion is given in the fifth section.

2. Segmentation

In this paper, we used an automatic segmentation algorithm based on Ant Colony optimization (ACO) [13,14]. It is an optimization algorithm inspired by the natural behavior of real ants. It consists of a number of ants (nodes) moving on an image seen as a multidimensional graph to identify pixels where an abrupt variation of intensity occurs. Ants' move is guided by the local intensity variation of the pixels and traces of the pheromone. At the end of the process, a map contours of the original image is established.

2.1. ACO algorithm

The stages followed by the ants while moving are illustrated by the following algorithm:

```
Radom initialization of K ants' position
    Initialization of pheromone matrix with an initial value τ0
        L=40, number of construction
    Construction of visibility matrix
    For eachiteration n=1 : N, do
        For each construction step l=1 : L, do
            For eachant k= 1 : K, do
                Random distribution of K ants
                Choose and go towards the next close pixel
                Update pheromone trail of visited pixel
            End
        End
        Update the visited pixels
    End
```

2.1.1. Process of initialiazation

Initially a matrix having the same size as the image is built. It is called initial matrix of traces of pheromones « τ_0». In all its positions (pixel),the same pheromone value (between 0 and 1)is added. Each ant is assigned a random position (pixel)on the image which has a dimension M*M (Table 1).

Table 1
Stages of construction of the solution with ACO algorithm.

Parameter	Value chosen
Alpha (α)	1
Beta (β)	0.01
Rho (ρ)	0.001
Number of iteration(N)	07
Number of tants (K)	$\sqrt{imagearea}$
Number of mouvement of deplacement (L)	40
Epsilon (ε)	0.1

Table 2
Local configuration to calculate the variation of intensity to the pixel (i, j).

$I(I_{i-1,\,j-1})$	$I_{(i-1,\,j)}$	$I_{(i-1,\,j+1)}$
$I_{(i,\,j-1)}$	$I_{(i,\,j)}$	$I_{(i,\,j+1)}$
$I_{(i+1,\,j-1)}$	$I_{(i+1,\,j)}$	$I_{(i+1,\,j+1)}$

2.1.2. Construction of matrix of information (visibility)

Another matrix called matrix of visibility (heuristic information) is built containing the local variation of the values of intensity I between each pixel (i, j) of the image and its neighbors. The heuristic information of the pixel (i, j) is determined as follows:

$$n_{i,j} = \frac{Vc\left(I_{i,j}\right)}{\sum_{i=1}^{M}\sum_{j=1}^{M} Vc\left(I_{i,j}\right)} \tag{1}$$

$$\sum_{i=1}^{M}\sum_{j=1}^{M} Vc(Ii,\ j) \quad : \text{Normalization factor}$$

$V_C\,(I_{i,j})$: is a function which operates on the local group around the pixel in question, it depends on the variation of the values of intensity in the local group, it is computed as follows [6,8] (Table 2):

$$V_C(I_i,j) = |I_{i-1,j-1} - I_{i+1,j+1}| + |I_{i-1,j} - I_{i+1,j}| + |I_{i-1,j+1} - I_{i+1,j-1}| + |I_{i,j-1} - I_{i,j+1}| \tag{2}$$

2.1.3. Ants' move

The move of an ant from a pixel (i_1, j_1) to an adjacent one (i_2, j_2) follows a random rule.

The probability of transition to explore the other pixel is given by:

$$p^{(n)}(i_0,j_0) = \begin{cases} \dfrac{(\tau i,\, j^{(n-1)})^{\alpha} * (ni,\, j)^{\beta}}{\sum_{(i,\,j)\,\in\,\varphi(i0,j0)} (\tau i,\, j^{(n-1)})^{\alpha} * (ni,\, j)^{\beta}} & If(i,j) \in \varphi(i_{0,j} i_o, j_0) \\ 0 & \text{otherwise} \end{cases} \tag{3}$$

(n): Index of iteration;

$\tau_{i,j}^{\,(n-1)}$: Pheromone value of the pixel (i,j);

$\varphi(i_0, j_0)$: All pixels that correspond to the points (i, j);

$n_{i,j}$: Heuristic information of the pixel (i, j)also called visibility;

α: A constant between 0 and 1 that controls the influence of the pheromone;

β: A constant between 0 and 1 that controls the influence of heuristic information.

An ant can thus move toany adjacent pixel but the most recently used ones. To do so, each ant has a memory.

2.1.4. Update

After its move,anant adds an amount of pheromone on the pixel. This process is called local update and is defined as follows:

$$\tau_{i,j}(n+1) = (1-\rho) * \tau_{i,j}(n) + \rho \Delta\tau(i,j) \tag{4}$$

ρ: is a constant between 0 and 1, it is called coefficient of weakening of pheromone;

$$\Delta\tau(i,j) = \frac{1}{ni,\,j} \tag{5}$$

At the end of process of construction « L » another update (total update)of the matrix of pheromone is carried. It is applied onpixels visited by at least one ant. This update is defined as follows:

$$\tau_{i,j}(n+1) = (1-\rho) * \tau_{i,j}(n) + \rho\tau_0(i,j) \tag{6}$$

2.1.5. Process of decision

It is the last step of detection of contours. The final matrix of pheromone built by the ants is used to make a decision on each pixel of the image. This decision enables us to say if a pixel belongs to the contour or not and to eliminate the pixels not contours.

This decision is binary; it is made for each pixel, by the application of threshold « T » on the final matrix of pheromone « τ(finale) ».

The decision is made after the application of a threshold on the final matrix of pheromone « τ(finale) ». The first step to select the threshold is to select T (0) as the median value of the final matrix of pheromone, thus, the values of the pheromone matrix are classified in two categories according to the criterion which a value is lower than T (0) or higher than T (0). Then, the new threshold is calculated like the average of two median values of each of two categories. This process is repeated until the threshold value does not change (in terms of tolerance defined by the user).

This process is detailed in the following:

Step1 : initialisationofT(0)

$$T(0) = \frac{\sum_{i=1}^{M}\sum_{j=1}^{M}\tau_{i,j}^{(final)}}{M^{*}M} \tag{7}$$

Step 2: Separate the pheromonematrix τ (final) in two classes, where the first is lower than T (l) and the second class is higher than this value.

After, we computethe average of each of the two classes as follows:

$$m_{L}^{(l)} = \frac{\sum_{i=1}^{M}\sum_{j=1}^{M} g_{T(l)}^{L}\tau_{i,j}^{(final)}}{\sum_{i=1}^{M}\sum_{j=1}^{M} h_{T(l)}^{L}\tau_{i,j}^{(final)}} \tag{8}$$

$$m_{U}^{(l)} = \frac{\sum_{i=1}^{M}\sum_{j=1}^{M} g_{T(l)}^{U}\tau_{I,j}^{(final)}}{\sum_{i=1}^{M}\sum_{j=1}^{M} h_{T(l)}^{U}\tau_{I,j}^{(final)}} \tag{9}$$

$$m_{U}^{(l)} = \frac{\sum_{i=1}^{M}\sum_{j=1}^{M} g_{T(l)}^{U}\tau_{I,j}^{(final)}}{\sum_{i=1}^{M}\sum_{j=1}^{M} h_{T(l)}^{U}\tau_{I,j}^{(final)}} \tag{10}$$

Where:

$$g_{T(l)}^{L}(x) = \begin{cases} xifx \le T(l) \\ 0otherwise \end{cases} \tag{11}$$

$$h_{T(l)}^{L}(x) = \begin{cases} 1ifx \le T(l) \\ 0otherwise \end{cases} \tag{12}$$

$$g_{T(l)}^{U}(x) = \begin{cases} xifx \ge T(l) \\ 0otherwise \end{cases} \tag{13}$$

$$h_{T(l)}^{U}(x) = \begin{cases} 1 & ifx \ge T(l) \\ 0 & otherwise \end{cases} \tag{14}$$

Step 3: Update the value of T (l)

$$T(l) = \frac{m_{L}^{(l)} - m_{U}^{(l)}}{2} \tag{15}$$

Step 4: Compare the value of T (l) between two successive iterations:

$$|T(1) = T(1-l)| > \varepsilon \tag{16}$$

ε: is a constant chosen by the user;

If this condition is satisfied, then we return tostep 2, else we stop. At this step the decision for each pixel is taken, whether it is a contour or not contour.

$$Ei,j = \begin{cases} 1 & if\tau i,j(N) \ge T(l) \\ 0 & otherwise \end{cases} \tag{17}$$

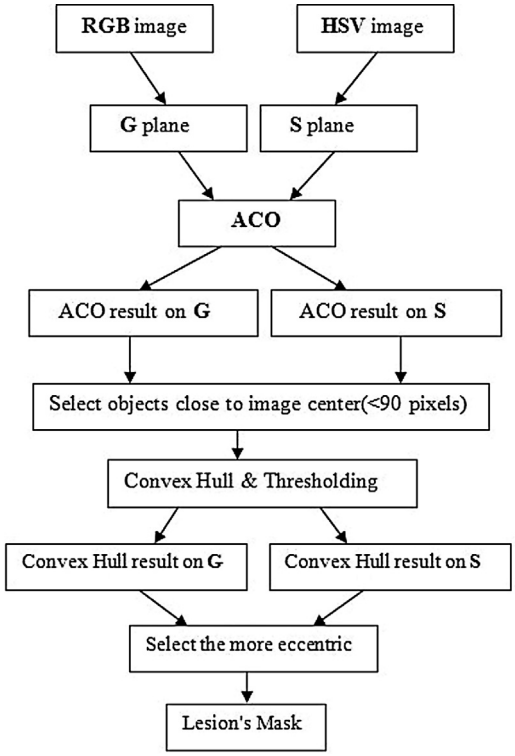

Fig. 1. The Proposed Algorithm.

Table 3
Selected features.

Feature	Signification	Related to:
$F4 = \frac{4\pi A}{L_1 p}$	Circularity	Shape feature
$F11 = \frac{B_3}{B_4}$	The ration between B_3 and B_4	Shape feature
F75	Minimum of the pixels intensities inside the lesion of the Rplan	Color variation feature
F76	Mean of the pixels intensities inside the lesion of the R, G and B plan	Color variation feature
F79	Maximum of the pixels intensities inside the lesion of theG plan	Color variation feature
F82	Maximum of the pixels intensities inside the lesion of the B plan	Color variation feature
F84	mean of the pixels intensities inside the lesion of the B plan	Color variation feature
F85	variance of the pixels intensities inside the lesion of the B plan	Color variation feature
F90	maximum of the pixels intensities inside the lesion of the S plan	Color variation feature
F94	Maximum of the pixels intensities inside the lesion of the V plan.	Color variation feature
$F100 = \frac{Rm}{Bm}$	Ratios between the intensities mean inside lesion of the R and B plan	Color variation feature
$F101 = \frac{Gm}{Bm}$	Ratios between the intensities mean inside lesion of the G and B plan	Color variation feature

2.2. The proposed algorithm

The ACO algorithm is applied on each plane of the three color system (RGB, HSV and LAB) and the grayscale image. The results show that best contours detection are obtained using green plane (G) and saturation plane (S). Both results are selected. The following algorithm showed in Fig. 1 presents the different steps of the segmentation algorithm.Then, the parameters used in the ACO algorithm are defined in the Table 3.

All objects that have an area greater than 10 pixels and have the distances from its Centroid to the center of image inferior to 90 are kept.

The ACO algorithm results are presented in the following figure, it shows the results obtained using green plane (G) and saturation plane (S).

Then, convex hull algorithm is used to envelope the objects, giving a convex hull mask shown in Fig. 3(a). Then the histogram is computed from the green plan (G) on pixels selected by the convex hull mask. The threshold in computed as the minimum that separates two peaks in the histogram (Fig. 5). If the histogram shows one peak the convex hull mask is considered as the final mask (Fig. 6). The different steps to find the final lesion mask of the bottom image shown in Fig. 2 are presented in Fig. 3.

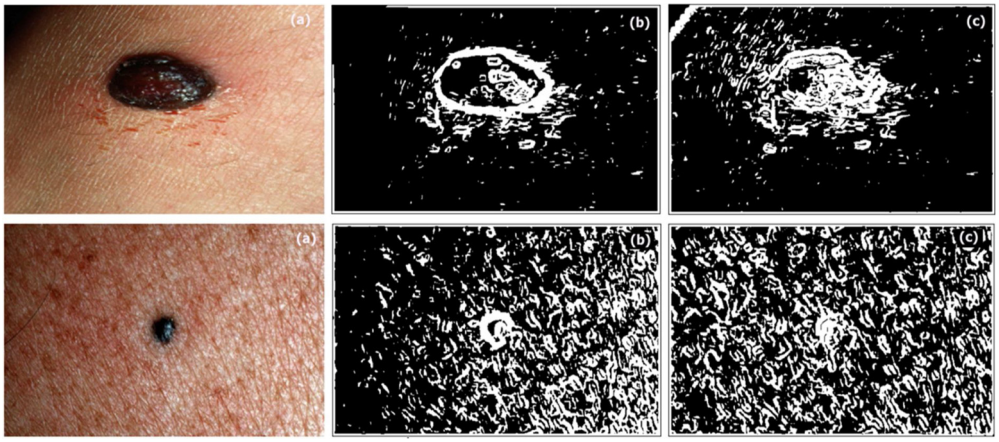

Fig. 2. The proposed algorithm result: (a): Original image. (b) Result of S plan. (c) Result of (G) plan.

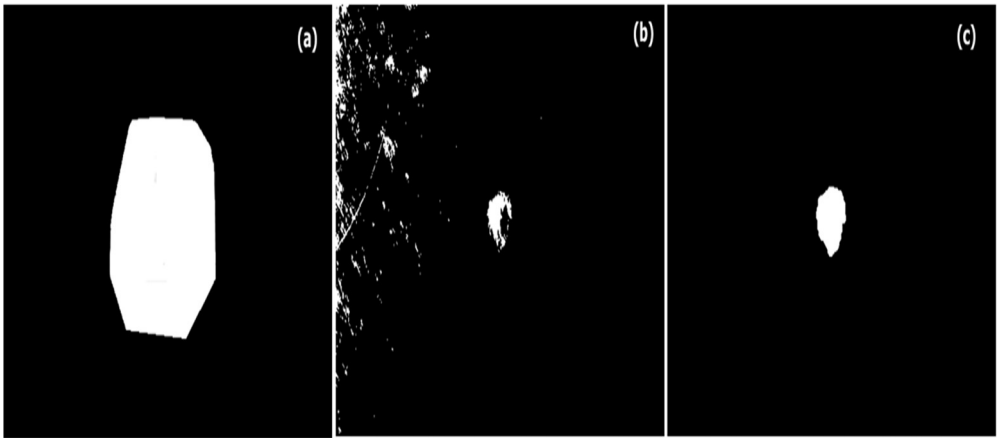

Fig. 3. Post processing segmentation: (a): Convex hull. (b) Thresholding. (c) Dilate filtering.

Fig. 4. Manual borders shown in red; proposed algorithm borders are denoted in dotted blue line. (For interpretation of the references to colour in this figure legend, the reader is referred to the web version of this article.)

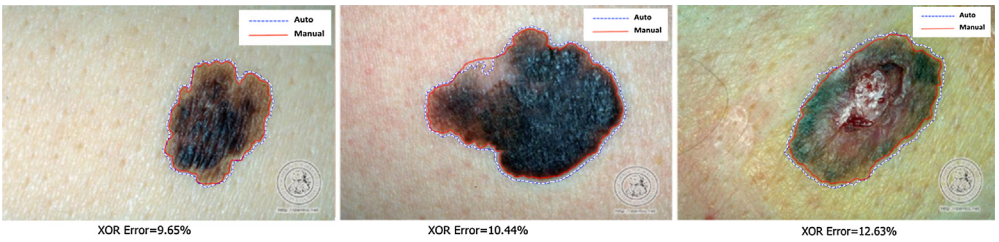

Fig. 5. Errors less than 13%. Manual borders shown in red; automatic borders are denoted in dotted blue line. (For interpretation of the references to colour in this figure legend, the reader is referred to the web version of this article.)

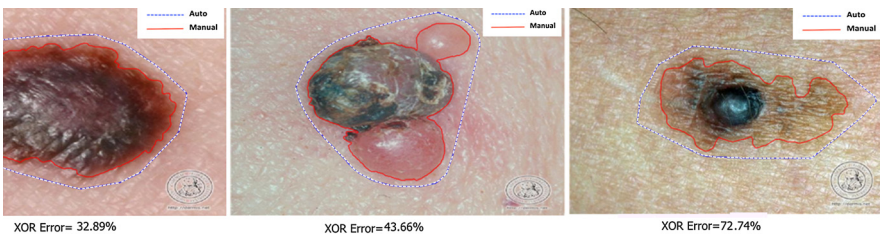

Fig. 6. Errors bigger than 30%. Manual borders shown in red; automatic borders are denoted in dotted blue line. (For interpretation of the references to colour in this figure legend, the reader is referred to the web version of this article.)

Fig. 4 shows the overlay manual contour (red) and the contour defined by the proposed algorithm (blue) (bottom image shown in Fig. 2).

2.3. Segmentation results

The set of images on which we tested our algorithm consists of 172 dermoscopic images, where, 88 are melanoma and 84 are benign. The images were extracted from the public databases (DermIS and DermQuest), with manual segmentation of each lesion. Manual masks are obtained from the expert and XOR error metric is used:

$$XORError = \frac{Auto\ Mask\ XOR\ ManualMask}{Manual\ Mask} \tag{18}$$

Figs. 5 and 6 show images for which the XOR errors of segmentation are less than 13% and greater than 30% respectively.

The average XOR Error of 172 images is 57.56% where the median is 17.48%. Using second validation metric, the Dice Similarity Coefficient [15], the DSC average Error is 0.8604, the DSC median is 0.8967.

3. Feature extraction

The extraction features are based on the geometrical properties, texture and relative color.

3.1. Shape features

The inhomogeneous growth of the tumor cells result on an expected form of lesion. The extracted features that characterize the shape of lesion are:

a) Solidity (F1): the ratio between the lesion area (A) and its convex hull area [16].

$$F1 = \frac{A}{ConvexHullArea} \tag{19}$$

b) Extent (F2): the ratio between the lesion area and its bounding box area [12]:

$$F2 = \frac{A}{Bounding\ \ BoxArea} \tag{20}$$

c) Equivalent diameter (F3) [16,17]:

d)

$$F3 = \frac{3A}{L_1 \pi} \tag{21}$$

Where L_1 is the length of the major axis passing through lesion center

e) Circularity (F4) [16]:

$$F4 = \frac{4\pi A}{L_1 p} \tag{22}$$

Where p is the lesion perimeter

f) The ratio between the principal axes (F5) [16,17]:

$$F5 = \frac{L_2}{L_1} \tag{23}$$

Where L_1 is the length of the major axis passing through lesion center and L_2 is the length of the minor axis, orthogonal to L_1 and passing through lesion center.

g) The ratio between the two sides of the lesion bounding box (F6) [16]:

$$F6 = \frac{L_2}{L_1} \tag{24}$$

h)The ratio between the lesion perimeter p and its area A (F7) [18]:

$$F7 = \frac{A}{p} \tag{25}$$

i)Where, B_1 and B_2 are the areas in each side of major axis L_1, (F8) is defined as [17]:

$$F8 = \frac{(B_1 - B_2)}{A} \tag{26}$$

j) Where, B_3 and B_4 are the areas in each side of axis L_2, F9 is similar to F8, but uses the shorter axis L_2 [18]:

$$F9 = \frac{(B_3 - B_4)}{A} \tag{27}$$

k) F10 is the ration between B_1 and B_2:

$$F10 = \frac{B_1}{B_2} \tag{28}$$

l) F11 is similar to F10, but makes use of the shorter axis L_2 [17]:

$$F11 = \frac{B_3}{B_4} \tag{29}$$

m) Boundary Irregularity features:

The F12 to F67 are quantifying the border irregularity [17], these features are calculated after computing the gradient of R, G and B plan, dilating the mask of lesion and selecting the pixels on the gradient corresponded to contour of the dilated mask of the three plans (R, G and B);

F12, F13, and F14: are the averages of selected pixels on the R, G, and B plan successively.

F15, F16 and F17: are the variances of the selected pixels on the R, G, and B plan successively;

Then, the lesion is divided on eighth slice [4,10];

F18 to F42: are the averages of selected pixels on the R, G, and B plan successively in each slice (3*8 features);

F43 to F67: are the variances of the selected pixels on the H, S, and V plan successively each slice (3*8 features);

3.2. Texture features

Six measurements (F68-F73) texture-based features are extracted from lesion. Their objective is to characterize the texture of the lesion. The extracted features include Mean, Standard Deviation, Skewness, energy, Entropy and Roughness [19,20].

a) Mean: It shows the value around which the dispersion occurs.

$$m = \frac{1}{n}\sum_{i=i}^{n} PxlL(i) \tag{30}$$

PxlL: Vector lesion pixels

b) Standard deviation: shows the variations of the pixels of image.

$$SdVar = \sqrt{\sum_{i=i}^{n} (PxlL(i) - m)^2} \tag{31}$$

c) Skewness: describes the level of asymmetry of a distribution around the mean

$$S = \left(\frac{1}{SdVar^3}\right)\sum_{i=i}^{n}(PxlL(i) - m)^3 \tag{32}$$

d) Energy

$$E = \sum_{i=i}^{n}(PxlL(i))^2 \tag{33}$$

e) Entropy: shows the degree of thehomogeneity pixels in the image.

$$Ep = -1\left(\sum_{i=1}^{n}(PxlL(i)\log(PxlL(i))\right) \tag{34}$$

f) Roughness:

$$R = 1 - \left(\frac{1}{1 + SdVar^2}\right) \tag{35}$$

3.3. Color features

Their goal is to quantify the color variation and the relative color in the lesion.

a) Color variation

Their goal is to quantify the color variation in the lesion. The selected features are:

F74-F85: maximum, minimum, mean and variance of the pixels intensities inside the lesion of the R, G and B plan [21].

F86-98: After converting the RGB image to HSV color system, the maximum, minimum, mean and variance of the pixels intensities inside the lesion of the H, S and V plan are defined.

F99-F102: Ratios between the intensities mean inside lesion of the R, G and B plan:

$$\mathrm{F99} = \frac{\mathrm{Rm}}{\mathrm{Gm}} \tag{36}$$

$$\mathrm{F100} = \frac{\mathrm{Rm}}{\mathrm{Bm}} \tag{37}$$

$$\mathrm{F101} = \frac{\mathrm{Gm}}{\mathrm{Bm}} \tag{38}$$

$$\mathrm{F102} = \frac{\mathrm{Gm}}{\mathrm{Rm}} \tag{39}$$

Where: Rm, Gm, Bm are the intensities mean inside lesion of the R, G and B plan respectively.

b) Relative color

It allows enhancing the differentiation of the malignant and benign lesions [22]. Considering color intensities inside and outside lesion:

$$\mathrm{F103} = \frac{\mathrm{ROut} - \mathrm{RL}}{\mathrm{RL} + \mathrm{GL} + \mathrm{BL}} \tag{40}$$

$$\mathrm{F104} = \mathrm{abs}\frac{\mathrm{GOut} - \mathrm{GL}}{\mathrm{RL} + \mathrm{GL} + \mathrm{BL}} \tag{41}$$

$$\mathrm{F105} = \mathrm{abs}\frac{\mathrm{BOut} - \mathrm{BL}}{\mathrm{RL} + \mathrm{GL} + \mathrm{BL}} \tag{42}$$

$$\mathrm{F106} = \frac{\mathrm{RL}}{\mathrm{RL} + \mathrm{GL} + \mathrm{BL}} \tag{43}$$

$$\mathrm{F107} = \frac{\mathrm{GL}}{\mathrm{RL} + \mathrm{GL} + \mathrm{BL}} \tag{44}$$

$$\mathrm{F108} = \frac{\mathrm{GL}}{\mathrm{RL} + \mathrm{GL} + \mathrm{BL}} \tag{45}$$

where

R_L, G_L, B_L: lesion average in red, green and blue plan.

R_{out}, G_{out}, B_{out}: outside lesion average in red, green and blue plan.

c) Color asymmetry

Table 4
The results of classification using KNN.

	Melanoma(88)	*Benign(84)*
Melanoma (88)	75 (85.22%)	13 (14.78%)
Benign (84)	13 (16.67.%)	70 (83.33%)

The image is subdivided into blocks. We measure the color distance between two symmetrical blocks along the two principal symmetrical axes, computing number of the asymmetrical and symmetrical blocks [10]. Measuring four features: F109-110 according to the vertical axis and F111-F112 according to the horizontal axis.

3.4. Feature selection

In the aim to select the most pertinent features to use for the learning and classification steps, we used Reliefalgorithm developed by Kira and Rendell [22] to estimates ranks and weights of the extracted features.

The description of Relief algorithm is given in the following table:

Input: for each training instance a vector of attribute values and the class value

Output: the vector W of estimations of the qualities of attributes

Set all weights W [A]: = 0.0;

For i: = 1 **to** m, **do**

Randomly select an instance R_i;

Find nearest hit H and nearest miss M;

For A: =1 **to** a, **do**

W [A]:=W [A]-diff (A, R_i, H)/m+diff (A,R_i,M)/m;

End

End

Pseudo code of the basic Relief algorithm.

Using the Relief algorithm [22] in order to select features which gives the best results of classification, 12 features were selected from the 112 extracted ones. And, for the 12 selected features, 10 features are related to the color variation ones (83%). The selected features are: F4, F11, F75, F76, F79, F82, F84, F85, F90, F94, F100 and F101.

These features are defined in the following table):

4. Classification

The selected features are used as input in two classifiers. In this study we used two classifiers:

- K Nearest Neighbor (KNN) method which gathers closest objects measuring the Standard Euclidian distance of normalized features. K is the number of neighbors and to differentiate malignant melanoma from benign lesion [23–25].
- Artificial Neural Network (NN). Both classifiers uses features extracted using manual and automatic masks (proposed algorithm segmentation).

In order to evaluate the automated system that uses an Ant colony based segmentation algorithm, the manual masks for each lesion are used.

4.1. Classification using the proposed algorithm based on ACO masks

For each lesion to classify, two classifiers K-Nearest Neighbor (KNN) and Artificial Neural Network (ANN) are tested using the masks given by an automated system that uses an Ant colony based segmentation algorithm.

4.1.1. The results of classification using KNN

To classify each lesion, the rest of lesion in dataset is considered as a training set. Fixing k = 3 the results are (Table 4):

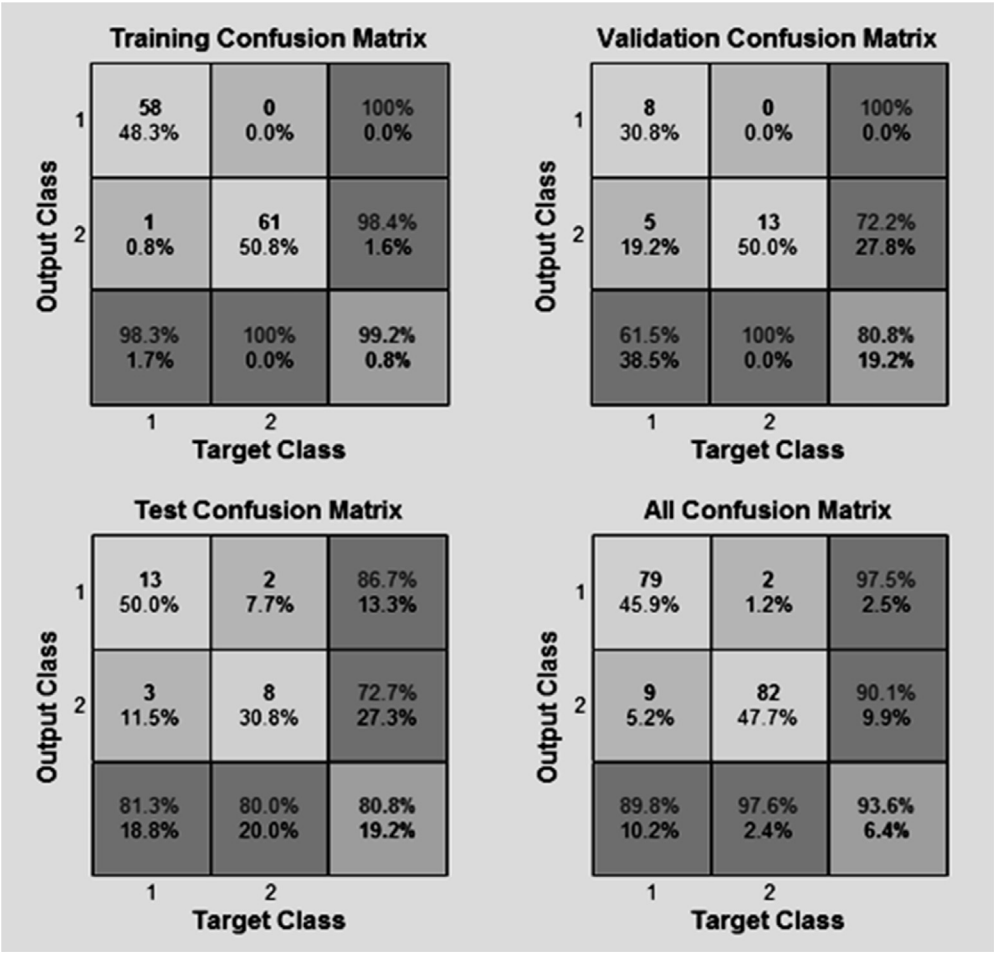

Fig. 7. Confusion matrix segmentation with automatic masks.

Table 5
The results of classification using KNN.

	Melanoma 88	Benign 84
Melanoma	77 (87.50%)	11 (12.50%)
Benign	17 (20.23%)	67 (79.75%)

4.1.2. The results of classification using ANN

Fig. 7 shows the results of classification using ANN:

The confusion matrix shows that the algorithm classified correctly 93.60% of the images.

4.2. Classification using manual masks

In order to evaluate the classification results given by the proposed algorithm based on ACO, the two classifiers K-Nearest Neighbor (KNN) and Artificial Neural Network (ANN) are tested using the manual masks.

4.2.1. The results of classification using KNN

The results of classification using manual masks and KNN are given in the following table (Table 5):

4.2.2. The results of classification using ANN

Fig. 8 shows the results of classification using ANN.

The confusion matrix shows that algorithm achieves 86.60% correctly classified.

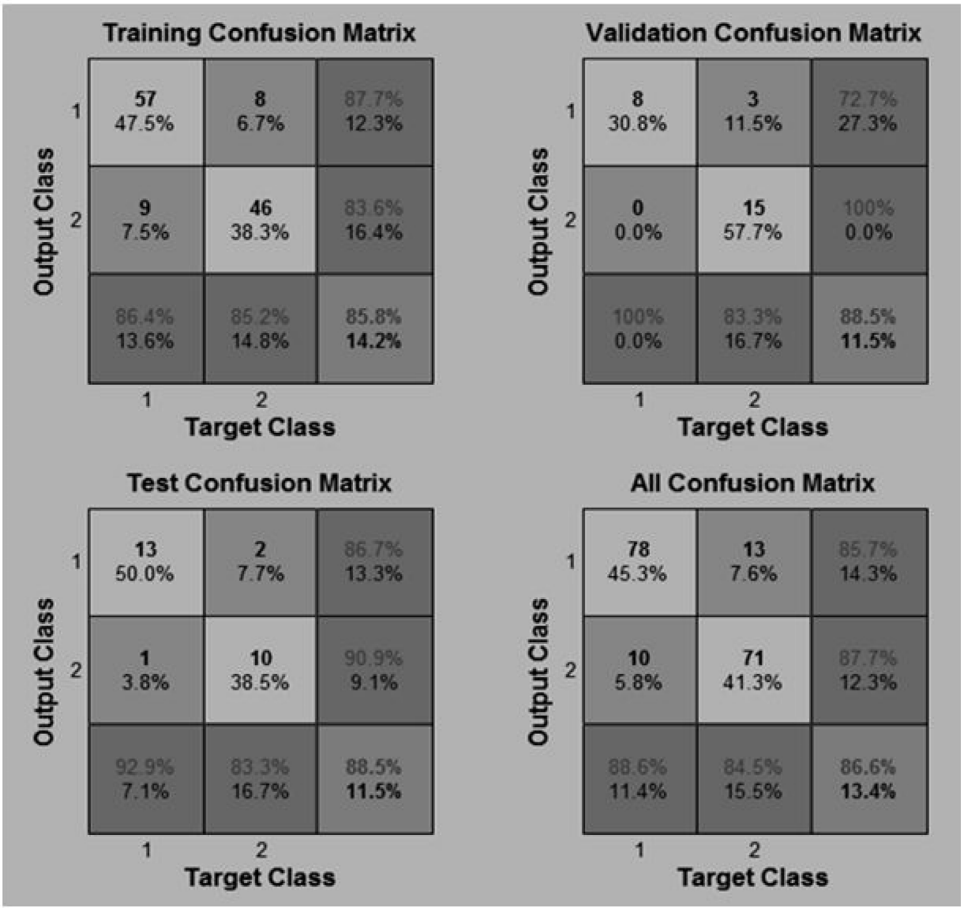

Fig. 8. Confusion matrix segmentation with manual masques.

4.3. Discussion

The results of the proposed system that uses an Ant colony based segmentation algorithm, taking into consideration three types of features to describe malignant lesion are very satisfactory. By using this algorithm, the edges can be observed inside lesions and the lesions contours are better detected than the manual masks. Knowing a priori that the most homogeneous part in the image is a legion and the lesion is relatively centered in the image, ACO detects most edges (objects) inside lesion. The convex Hull allows gathering the objects that constituted the lesion, and then the histogram refines the localization of the lesion. In some image the lesion are difficult to detect because of weak border of lesion, as mentioned in [26] and [27]. The classification results, using neural network show that, the automatic segmentation provides better results than the manual one. Using automatic masks allows to classify 93.60% of images correctly against 86.60% for manual masks.

Based on the colors, textures and geometrical features lead to a misclassification of some lesions, an additional feature as a structures of melanoma (dots, Blue-white veil, steak...) are need to improve the classification.

5. Conclusion

The aim of the study is to identify, automatically, melanoma from benign lesions. Based on image processing techniques the efficiency of the proposed segmentation algorithm is tested, most pertinent features that describe melanomas are extracted. The set of features are reduced by selecting the most pertinent ones. The automated system is tested on 172 dermoscopic images where 88 are malignant melanomas and 84 benign lesions. K-Nearest Neighbors classified 85.22% of tested images correctly against 87.50% for manual masks. Neural Network classified correctly 93.60% of tested images with automatic masks against 86.60% for manual masks. The results show that the selected features are promising.

References

[1] A.W. Kopf, T.G. Salopek, J. Slade, A.A. Marghoob, R.S. Bart, Techniques of cutaneous examination for the detection of skin cancer, Cancer 75 (S2) (1995) 684–690.
[2] D.M. Parkin, F. Bray, J. Ferlay, P. Pisani, Global cancer statistics, 2002, CA Cancer J. Clin. 55 (2) (2005) 74–108.
[3] R.L. Siegel, K.D. Miller, A. Jemal, Cancer statistics, 2015, CA. Cancer J. Clin. 65 (1) (2015) 5–29.
[4] W. Stolz, A. Riemann, A. Cognetta, L. Pillet, W. Abmayr, D. Holzel, P. Bilek, F. Nachbar, M. Landthaler, Abcd rule of dermatoscopy-a new practical method for early recognition of malignant-melanoma, Eur. J. Dermatol. 4 (7) (1994) 521–527.
[5] F. Nachbar, W. Stolz, T. Merkle, A.B. Cognetta, T. Vogt, M. Landthaler, P. Bilek, O. Braun-Falco, G. Plewig, The abcd rule of dermatoscopy: high prospective value in the diagnosis of doubtful melanocytic skin lesions, J. Am. Acad. Dermatol. 30 (4) (1994) 551–559.
[6] G. Argenziano, C. Catricalà, M. Ardigo, P. Buccini, P. De Simone, L. Eibenschutz, A. Ferrari, G. Mariani, V. Silipo, I. Sperduti, Seven-point checklist of dermoscopy revisited, Br. J. Dermatol. 164 (4) (2011) 785–790.
[7] I. Zalaudek, G. Argenziano, H. Soyer, R. Corona, F. Sera, A. Blum, R. Braun, H. Cabo, G. Ferrara, A. Kopf, Three-point checklist of dermoscopy: an open internet study, Br. J. Dermatol. 154 (3) (2006) 431–437.
[8] J.S. Henning, S.W. Dusza, S.Q. Wang, A.A. Marghoob, H.S. Rabinovitz, D. Polsky, A.W. Kopf, The cash (Color, architecture, symmetry, and homogeneity) algorithm for dermoscopy, J. Am. Acad. Dermatol. 56 (1) (2007) 45–52.
[9] M. Rastgoo, R. Garcia, O. Morel, F. Marzani, Automatic differentiation of melanoma from dysplastic nevi, Comput. Med. Imaging Graph. 43 (2015) 44–52.
[10] R. Kasmi, K. Mokrani, Classification of malignant melanoma and benign skin lesions: implementation of automatic abcd rule, IET Image Proc. 10 (6) (2016) 448–455.
[11] L.K. Ferris, J.A. Harkes, B. Gilbert, D.G. Winger, K. Golubets, O. Akilov, M. Satyanarayanan, Computer-aided classification of melanocytic lesions using dermoscopic images, J. Am. Acad. Dermatol. 73 (5) (2015) 769–776.
[12] R. LeAnder, P. Chindam, M. Das, S.E. Umbaugh, Differentiation of melanoma from benign mimics using the relative-color method, Skin Res. Technol. 16 (3) (2010) 297–304.
[13] M. Dorigo, M. Birattari, T. Stutzle, AntColonyOptimization, IEEE Comput. Intell. Mag. 1 (4) (2006) 28–39.
[14] M. Dorigo, V. Maniezzo, A. Colorni, Ant system: optimization by a colony of cooperating agents, IEEE Trans. Syst. Man Cybern. Part B (Cybern.) 26 (1) (1996) 29–41.
[15] K.H. Zou, S.K. Warfield, A. Bharatha, C.M. Tempany, M.R. Kaus, S.J. Haker, W.M. Wells, F.A. Jolesz, R. Kikinis, Statistical validation of image segmentation quality based on a spatial overlap index 1: scientific reports, Acad. Radiol. 11 (2) (2004) 178–189.
[16] J.F. Alcón, C. Ciuhu, W. Ten Kate, A. Heinrich, N. Uzunbajakava, G. Krekels, D. Siem, G. De Haan, Automatic imaging system with decision support for inspection of pigmented skin lesions and melanoma diagnosis, IEEE J. Sel. Top. Signal Process. 3 (1) (2009) 14–25.
[17] P.G. Cavalcanti, J. Scharcanski, Macroscopic pigmented skin lesion segmentation and its influence on lesion classification and diagnosis, in: Color Medical Image Analysis, Springer, 2013.
[18] T. Fikrle, K. Pizinger, Digital computer analysis of dermatoscopical images of 260 melanocytic skin lesions; Perimeter/Area ratio for the differentiation between malignant melanomas and melanocytic nevi, J. Eur. Acad. Dermatol. Venereol. 21 (1) (2007) 48–55.
[19] R.M. Haralick, K. Shanmugam, Textural features for image classification, IEEE Trans. Syst. Man Cybern. 3 (6) (1973) 610–621.
[20] O. Marques, Practical Image and Video Processing Using Matlab, John Wiley & Sons, 2011.
[21] J.F. Alcón, C. Ciuhu, W. Ten Kate, A. Heinrich, N. Uzunbajakava, G. Krekels, D. Siem, G. De Haan, Automatic imaging system with decision support for inspection of pigmented skin lesions and melanoma diagnosis, IEEE J. Sel. Top. Signal Process. 3 (1) (2009) 14–25.
[22] K. Kira, L.A. Rendell, The feature selection problem: traditional methods and a new algorithm, Aaai (1992).
[23] B.V. Dasarathy, Nearest Neighbor ({Nn}) Norms:{Nn} Pattern Classification Techniques, 1991.
[24] H. Ganster, P. Pinz, R. Rohrer, E. Wildling, M. Binder, H. Kittler, Automated melanoma recognition, IEEE Trans. Med. Imaging 20 (3) (2001) 233–239.
[25] A.A. Safi, Towards Computer–Aided Diagnosis of Pigmented Skin Lesionson, Citeseer, 2012, 2017.
[26] M. Emre Celebi, Q. Wen, S. Hwang, H. Iyatomi, G. Schaefer, Lesion border detection in dermoscopy images using ensembles of thresholding methods, Skin Res. Technol. 19 (1) (2013) e252–e258.
[27] R. Kasmi, K. Mokrani, R. Rader, J. Cole, W. Stoecker, Biologically inspired skin lesion segmentation using a geodesic active contour technique, Skin Res. Technol. (2015).